JOURNAL OF COATING TECHNOLOGY AND INNOVATION
Oct-Dec 2025, VOL. 3, ISSUE 4, pp. 1-7
https://doi.org/10.61577/jcti.2025.1000016

RESEAPRO JOURNALS

ORIGINAL ARTICLE

OPEN ACCESS

TiO_2 - graphene reinforced epoxy coatings for enhanced wear and corrosion protection

Vikram Kedambadi Vasu

Centre for Additive Manufacturing, Department of Mechanical Engineering, Nitte (Deemed to be University), Nitte Meenakshi Institute of Technology, Bengaluru, Karnataka, India

ABSTRACT

Developing durable multifunctional coatings is essential for protecting metal substrates exposed to combined mechanical and corrosive environments, where conventional epoxy systems often fail due to limited hardness and inadequate long-term barrier performance. This study develops TiO_2–Graphene reinforced epoxy coatings on Al6061 alloy using a sol–gel assisted dip-coating method to harness the complementary advantages of ceramic rigidity and graphene's impermeable network. The influence of TiO_2 (0.5–2 wt.%) and graphene (0.1–0.5 wt.%) was evaluated through XRD, SEM-EDS, surface profilometry, microhardness testing, pin-on-disc tribology (ASTM G99), and electrochemical measurements (PDP and EIS) in 3.5 wt.% NaCl. The hybrid coating (E–TiGr) exhibited a dense, defect-free microstructure with uniform nanoscale dispersion, resulting in a hardness increase from 21.6 HV (neat epoxy) to 42.1 HV. Wear rate decreased from 1.28×10^{-4} to 0.51×10^{-4} $mm^3 \cdot N^{-1} \cdot m^{-1}$, accompanied by a lower coefficient of friction (0.41). Electrochemical tests showed a shift toward a more positive corrosion potential (–0.588 V) and a reduced corrosion current density (1.1×10^{-6} $A \cdot cm^{-2}$), corresponding to ~72% protection efficiency. EIS confirmed the highest charge-transfer resistance (~5.8 $k\Omega \cdot cm^2$), indicating restricted ionic transport. Overall, the TiO_2–Graphene hybrid epoxy coating demonstrates significantly improved mechanical integrity and corrosion resistance, highlighting its potential for marine, automotive, and structural applications.

KEY WORDS

Hybrid coatings; TiO_2-Graphene; Epoxy nanocomposite; Sol–gel dip-coating; Corrosion and wear resistance

ARTICLE HISTORY

Received 28 October 2025; Revised 17 November 2025; Accepted 25 November 2025

Introduction

Metallic components used in industrial, marine, and transportation sectors are often exposed to harsh environments that induce both electrochemical corrosion and mechanical degradation. The inherent thermodynamic instability of metals in oxidative atmospheres makes corrosion an unavoidable phenomenon, while mechanical actions such as abrasion, erosion, and sliding wear further accelerate surface damage [1, 2]. In combined service conditions, the synergy between wear and corrosion termed tribocorrosion can drastically shorten component life and increase maintenance costs [3]. Conventional surface treatments and single-phase coatings, although effective to some extent, often fail to provide simultaneous resistance against both chemical and mechanical attacks. For instance, purely ceramic coatings such as TiO_2 or Al_2O_3 offer excellent hardness and chemical inertness but suffer from brittleness, poor adhesion to ductile substrates, and susceptibility to cracking under load [4]. Conversely, polymeric coatings like epoxy and polyurethane exhibit good flexibility and adhesion but lack sufficient hardness, thermal stability, and long-term corrosion protection when exposed to aggressive electrolytes [5].

To overcome these limitations, hybrid ceramic-polymer coatings have emerged as an effective solution, combining the advantages of inorganic rigidity and organic flexibility within a single architecture [6,7]. The ceramic phase contributes to improved hardness, thermal resistance, and chemical stability, while the polymer phase enhances adhesion, toughness, and crack tolerance. Such synergy allows hybrid coatings to exhibit superior barrier properties, lower defect density, and enhanced durability compared to their monolithic counterparts [8]. Among the various hybrid systems, the incorporation of nanoceramic fillers like TiO_2 and functional carbon nanostructures such as graphene into polymer matrices has gained considerable attention in recent years [9]. TiO_2 nanoparticles provide mechanical reinforcement and photocatalytic stability, whereas graphene acts as a two-dimensional impermeable barrier that restricts the penetration of corrosive ions and simultaneously improves load transfer within the coating [10].

Building upon these advancements, the present research aims to develop and characterize a TiO_2–Graphene reinforced epoxy coating designed to offer dual protection against wear and corrosion. The combination of TiO_2 and graphene within an epoxy matrix is expected to produce a dense, adherent, and multifunctional surface layer capable of resisting electrochemical degradation while maintaining high mechanical integrity. The study systematically investigates the coating's microstructure, mechanical performance, and electrochemical behaviour, providing a detailed structure-property correlation that highlights its suitability for industrial applications such as marine structures, automotive components, and lightweight aerospace alloys. Based on the limitations of existing epoxy-based protective systems, the central research question of this study is whether the combined incorporation of TiO_2 nanoparticles and graphene nanosheets can produce a hybrid epoxy coating with superior mechanical integrity, wear stability, and corrosion resistance compared to single-filler systems. Accordingly, the aim of this work is to develop a TiO_2–Graphene reinforced epoxy coating using a sol–gel assisted dip-coating method and to systematically evaluate its structural, tribological, and electrochemical performance . By establishing structure–

***Correspondence:** Dr. Vikram Kedambadi Vasu, Assistant Professor, Centre for Additive Manufacturing, Department of Mechanical Engineering, Nitte (Deemed to be University), Nitte Meenakshi Institute of Technology, Bengaluru, Karnataka, India, email: vikramkv123@gmail.com

property relationships, the study seeks to demonstrate the synergistic reinforcement mechanism responsible for the multifunctional improvement of the hybrid coating.

Experimental Procedure

Materials and coating process

The coating system was developed using Al6061 alloy substrates, TiO_2 nanoparticles, graphene nanosheets, and a two-component epoxy binder. The Al6061 plates (50mm*25mm*5mm) were mechanically polished using successive grades of emery paper (400-1200 grit), ultrasonically cleaned in acetone, and finally dried at 60 °C for 30 min [11-12]. The TiO_2 nanopowder (30-50 nm, ≥99 % purity) and graphene nanosheets were procured from Ultrananotech Pvt Ltd, India, whereas the epoxy resin and hardener were obtained locally from ResiChem Bengaluru [13]. The chemical and supplier details are summarized in table 1.

Table 1. Materials used for TiO_2–Graphene–Epoxy hybrid coating.

Material	Key Specification	Function
Al6061 substrate	Si-Mg-Al alloy, 50*25*5 mm	Substrate
TiO_2 nanoparticles	30-50 nm, 99 % purity	Ceramic reinforcement
Graphene nanosheets	Conductive, < 5 µm lateral size	Barrier and load-transfer phase
Epoxy resin + hardener	Two-component, ambient-cure system	Polymeric binder

The experimental workflow adopted for hybrid coating deposition is illustrated in figure 1, outlining the sequential steps of TiO_2 dispersion, graphene mixing, epoxy blending, substrate cleaning, dip-coating, and curing. TiO_2 nanoparticles were first dispersed in ethanol using ultrasonication for 30 min, followed by gradual addition of graphene nanosheets under continuous mechanical stirring to achieve homogeneous suspension [14]. The mixed dispersion was blended into epoxy resin, and the hardener was added just before deposition to control pot life.

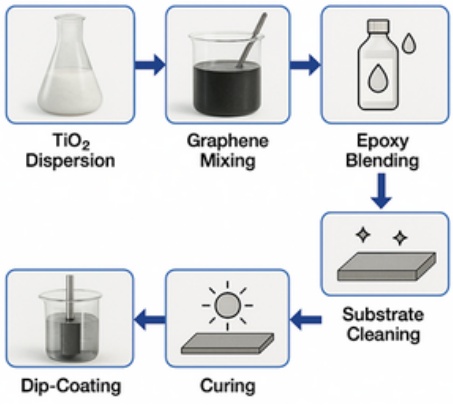

Figure 1. Schematic illustration of the TiO_2=Graphene-Epoxy hybrid coating process involving sol–gel dispersion, mixing, dip-coating, and thermal curing.

The cleaned Al6061 substrates were immersed vertically in the prepared hybrid resin bath and withdrawn at a controlled speed of 10 mm min^{-1} to ensure uniform film thickness [15]. Each coated specimen was air-dried for 30 min, followed by thermal curing at 120 °C for 2 h and post-curing at 150 °C for 1 h in a hot-air oven. The typical coating thickness after a single layer was ≈ 50 µm, which could be increased to ≈ 150 µm with multiple coats. The raw materials and coated specimen are shown in figure 2.2. TiO_2 appeared as a fine white powder, graphene nanosheets as dark flakes, and the epoxy resin as a translucent amber liquid. The coated Al6061 sample exhibited a uniform, glossy surface, confirming good wetting and adhesion after curing.

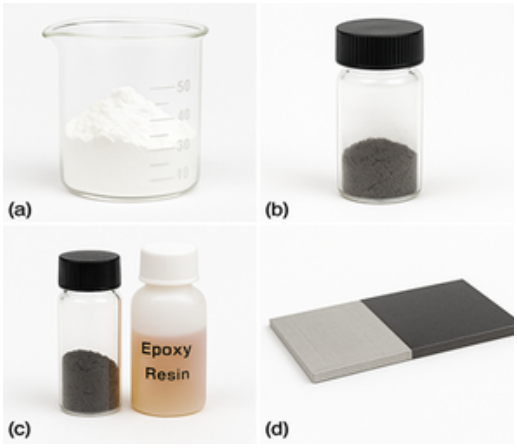

Figure 2. Coating materials and specimen: (a) TiO_2 nanopowder, (b) graphene nanosheets, (c) epoxy resin and hardener, (d) hybrid-coated Al6061 substrate.

Coating process parameters and experimental design

The performance of TiO_2–Graphene–Epoxy coatings is governed by deposition variables including filler loading, dispersion duration, withdrawal speed, and curing temperature [16]. A single-factor variation approach was adopted, optimizing each parameter while keeping others constant. TiO_2 content was varied between 0.5-2.0 wt.% and graphene between 0.1–0.5 wt.%. Ultrasonic dispersion (15-45 min) ensured effective de-agglomeration [17]. Dip-coating withdrawal speeds of 5-15 mm min^{-1} were evaluated to obtain uniform films without sagging. Curing involved a two-stage cycle: 100–130 °C for initial cross-linking and 140-160 °C for post-curing. After each trial, coating uniformity, adhesion, thickness, and roughness were assessed, and the optimized parameter ranges are summarized in Table 2.

Table 2. Process parameters considered for TiO_2–Graphene–Epoxy hybrid coating.

Parameter	Range Studied	Evaluation Criterion
TiO_2 loading (wt.%)	0.5 - 2.0	Surface uniformity, microhardness
Graphene loading (wt.%)	0.1 - 0.5	Barrier integrity, absence of agglomerates
Ultrasonic dispersion time	15 - 45 min	Homogeneity of suspension
Withdrawal speed	5 - 15 mm min^{-1}	Smooth coating flow, no streaking
Curing temperature (stage 1)	100 - 130 °C	Proper solvent removal
Post-curing temperature (stage 2)	140 - 160 °C	Enhanced adhesion and cross-linking
Number of coats	1 - 3	Thickness control and adhesion consistency

https://doi.org/10.61577/jcti.2025.1000016

The selected weight ratios of TiO_2 (1.0 wt.%) and graphene (0.3 wt.%) were based on preliminary optimization trials and supported by literature reports indicating that low ceramic loadings (0.5–2 wt.%) improve hardness and wear resistance without causing particle agglomeration [1, 3], while ultra-low graphene levels (0.1–0.5 wt.%) enhance barrier properties and load transfer without compromising dispersion stability [9,14]. The chosen combination provided the best balance of viscosity, dispersion quality, film uniformity, and mechanical response, and produced defect-free coatings during dip-coating. Higher loadings led to increased viscosity, agglomeration, and surface defects, whereas lower loadings showed insufficient reinforcement

Characterization techniques

A comprehensive set of structural, morphological, mechanical, and electrochemical characterizations was conducted under controlled ambient conditions (25 ± 2 °C, 50 ± 5 % RH). XRD analysis (Bruker D8 Advance, Cu Kα) was performed over 10°–80° (2θ) to confirm TiO_2 phase stability and detect crystalline changes within the hybrid matrix [18,19]. Surface morphology, elemental distribution, and cross-sectional features were examined using SEM–EDS (JEOL JSM-IT200) [20, 21]. Surface roughness and coating thickness were measured using a Mitutoyo SJ-210 profilometer [22, 24]. Microhardness was evaluated using a Vickers tester (100 g, 10 s) following ASTM E384 [25, 26]. Tribological behaviour was assessed using a Ducom TR-20LE pin-on-disc tribometer according to ASTM G99 (10 N, 0.2 m·s^{-1}, 1000 m) [27, 28]. Electrochemical corrosion performance in 3.5 wt.% NaCl was examined using an Autolab PGSTAT302N via PDP (–1.5 to +1.5 V, 1 mV·s^{-1}) and EIS (10^5–10^{-2} Hz, 10 mV AC) measurements [29, 30]. A complete summary of the equipment and test parameters is provided in Table 3.

Table 3. Equipment and testing parameters used for characterization.

Technique	Instrument (Model)	Standard / Parameter Range
X-ray diffraction (XRD)	Bruker D8 Advance	10°–80° (2θ), 0.02° step, Cu Kα
Scanning Electron Microscopy + EDS	JEOL JSM-IT200	10 kV accelerating voltage
Surface roughness / thickness	Mitutoyo SJ-210	Ra = 0.1–10 µm, cutoff = 0.8 mm
Microhardness	Shimadzu HMV-G21DT	100 g load, 10 s dwell
Tribology (pin-on-disc)	Ducom TR-20LE	ASTM G99, 10 N, 0.2 m/s
Electrochemical testing	Autolab PGSTAT302N	PDP/EIS, 3.5 wt.% NaCl

Sample coding and experimental workflow

For systematic analysis, all coating specimens were assigned specific codes based on the type and combination of nanofillers incorporated in the epoxy matrix. The coding nomenclature followed the convention "E-X," where E represents the epoxy matrix and X denotes the filler phase. The details of sample identification are summarized in table 4.

Table 4. Sample coding and composition of TiO_2-Graphene-Epoxy hybrid coatings.

Sample Code	Composition Description	Filler Content (wt.%)
E0	Neat epoxy coating (control)	0
E-Ti	Epoxy + TiO_2 nanoparticles	1.0
E-Gr	Epoxy + Graphene nanosheets	0.3
E-TiGr	Epoxy + TiO_2 (1.0 wt.%) + Graphene (0.3 wt.%)	1.3 (total)

Each coating formulation was fabricated under strictly controlled and identical experimental conditions to maintain reproducibility across all compositions. The deposition and curing stages were standardized for every specimen to ensure consistent film formation and interfacial bonding. Following thermal curing, the coated samples were carefully examined for surface uniformity, absence of defects such as pinholes or delamination, and overall adhesion quality. The experimental workflow was designed to follow a linear progression from material preparation and dispersion of nanofillers to coating application, curing, and subsequent performance evaluation ensuring that all comparative analyses were based on coatings produced under uniform processing environments.

Results and Discussions

X-ray diffraction (XRD) analysis

The The X-ray diffraction (XRD) patterns of the neat epoxy (E0), TiO_2-filled (E-Ti), graphene-filled (E-Gr), and hybrid (E-TiGr) coatings are shown in Figure 3.

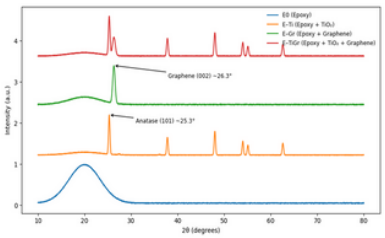

Figure 3. X-ray diffraction patterns of E0 (epoxy), E-Ti (epoxy + TiO_2), E-Gr (epoxy + graphene), and E-TiGr (epoxy + TiO_2 + graphene) coatings.

XRD patterns were recorded using a Bruker D8 Advance diffractometer (Cu Kα, 40 kV, 30 mA) over 10°–80° (2θ, 0.02° step). The neat epoxy (E0) showed a broad amorphous halo near 20°, characteristic of cross-linked polymers. The E–Ti coating exhibited distinct anatase TiO_2 peaks at 25.3°, 37.8°, 48.0°, 54.0°, and 62.6°, along with minor rutile reflections at 27.4° and 36.1°. The neat epoxy (E0) coating showed a broad amorphous halo near 20°, with a very weak trace peak arising from partially ordered polymer chain segments and microcrystalline domains formed during curing, which consistent with typical XRD signatures of cross-linked epoxy systems. The E–Gr sample displayed a weak (002) graphene peak at 26.3°, confirming partial graphitic ordering. In the hybrid E–TiGr coating, all TiO_2 and graphene peaks were retained with slight broadening, indicating uniform nanoscale dispersion, stable phase coexistence, and strong filler–matrix interaction consistent with the enhanced mechanical and corrosion performance.

Surface morphology and elemental composition (SEM-EDS analysis)

Figure 4(a) shows the neat epoxy (E0) surface, which appears smooth and featureless with minor voids typical of an unreinforced polymer film. In Figure 4(b), the TiO_2-filled coating (E–Ti) displays uniformly dispersed bright nanoparticle regions, indicating good particle–matrix adhesion and reduced porosity. The graphene coating (E-Gr) in Figure 4(c) exhibits wrinkled, layered features characteristic of exfoliated graphene sheets. The hybrid E–TiGr coating (Figure 4d) presents a compact, crack-free morphology where TiO_2 particles are anchored on

https://doi.org/10.61577/jcti.2025.1000016

graphene domains, forming a dense interconnected network that supports the observed improvements in bonding, compactness, and durability.

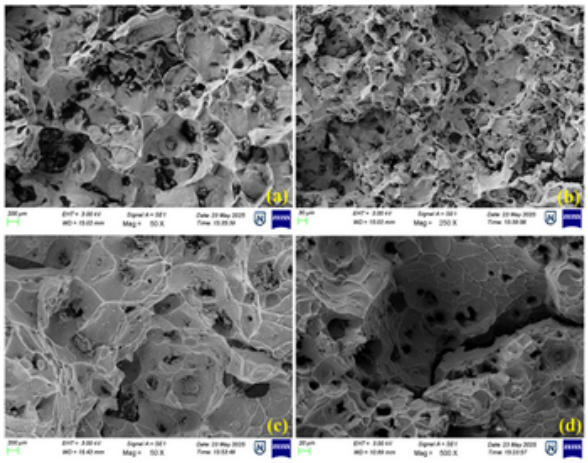

Figure 4. SEM micrographs of (a) E0, (b) E–Ti, (c) E–Gr, and (d) E–TiGr coatings.

Figure 5 presents the EDS spectra of the coatings. The neat epoxy (E0) shows dominant C Kα (0.28 keV) and O Kα (0.53 keV) peaks with a minor Al signal from the substrate, consistent with a thin polymer layer. The E–Ti sample displays clear Ti Kα (4.5 keV) and Ti Kβ (4.9 keV) peaks, confirming uniform TiO_2 incorporation. The graphene coating (E–Gr) exhibits an intensified carbon peak and reduced oxygen content, reflecting its high C/O ratio. In the hybrid E–TiGr coating, both Ti and C peaks persist, with slight Ti peak broadening indicating nanoscale confinement and strong interfacial interaction. Semi-quantitative EDS showed Ti ≈ 6.4 wt%, C ≈ 8.9 wt%, and O ≈ 12.7 wt%.

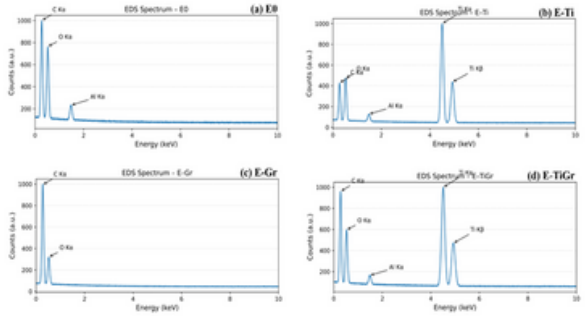

Figure 5. EDS spectra of (a) E0, (b) E-Ti, (c) E-Gr, and (d) E-TiGr coatings.

The weight ratios used in the coatings were 1.0 wt.% TiO_2 in E–Ti, 0.3 wt.% graphene in E–Gr, and a combined 1.0 wt.% TiO_2 + 0.3 wt.% graphene in the hybrid E–TiGr formulation. These compositions correspond to the filler loadings used in the EDS spectra presented in Figure 5.

Surface roughness and coating thickness evaluation

Surface roughness and coating thickness were evaluated using a Mitutoyo SJ-210 profilometer (4 mm scan length, 0.8 mm cutoff, 2 µm stylus), with values additionally verified from cross-sectional SEM. As shown in Figure 6, neat epoxy (E0) exhibited the lowest roughness (Ra ≈ 0.42 µm) and a thickness of ~43 µm. TiO_2 addition (E–Ti) increased roughness slightly (Ra ≈ 0.58 µm), whereas graphene (E–Gr) resulted in higher roughness (Ra ≈ 0.67 µm). The hybrid E–TiGr coating showed moderate roughness (Ra ≈ 0.61 µm) with the most uniform and highest thickness (~52 µm), indicating a compact and well-dispersed filler network that enhances coating integrity.

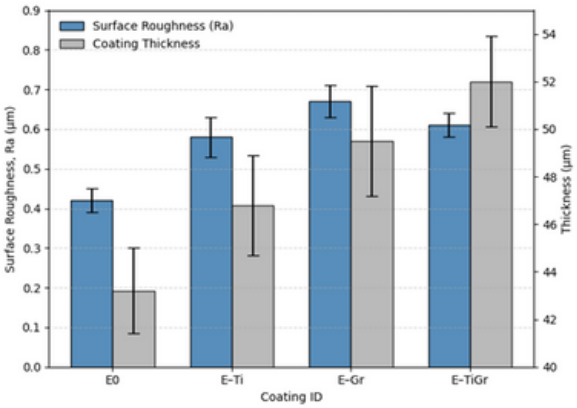

Figure 6. Variation in surface roughness (Ra) and coating thickness of E0, E–Ti, E–Gr, and E–TiGr coatings.

Microhardness evaluation

Microhardness testing was performed using a Shimadzu HMV-G21DT Vickers tester (100 g, 10 s, ASTM E384), with five valid indentations averaged for each coating.

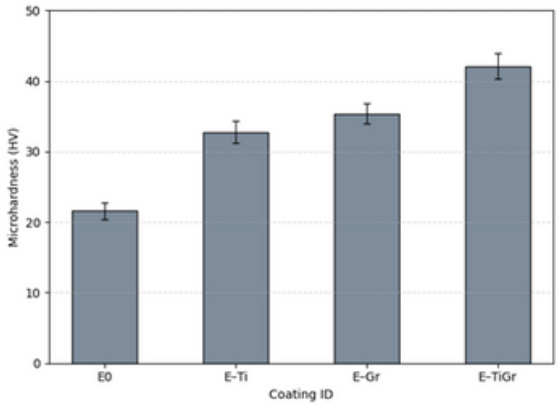

Figure 7. Variation in vickers microhardness of E0, E–Ti, E–Gr, and E–TiGr coatings.

As shown in Figure 7, neat epoxy (E0) exhibited the lowest hardness (~21.6 HV), reflecting its soft polymeric nature. TiO_2 reinforcement (E–Ti) increased hardness to ~32.8 HV due to the load-bearing effect of the ceramic nanoparticles, while graphene incorporation (E–Gr) further improved hardness to ~35.4 HV through enhanced stress distribution. The hybrid E–TiGr coating achieved the highest hardness (~42.1 HV), confirming the synergistic interaction between TiO_2 and graphene, which enhances compactness, interfacial bonding, and resistance to localized deformation.

Tribological performance (Wear and coefficient of friction analysis)

Tribological performance was evaluated using a Ducom TR-20LE pin-on-disc tribometer (ASTM G99) with a 6 mm EN31 steel pin under 10 N load, 0.2 $m \cdot s^{-1}$ sliding speed, and 1000 m distance. Wear volume was calculated from mass loss, and COF was recorded continuously. As shown in Figure 8, the neat epoxy (E0) showed the highest wear rate (1.28×10^{-4} $mm^3 \cdot N^{-1} \cdot m^{-1}$) and COF (0.64). TiO_2 reinforcement (E–Ti) reduced wear to 0.85×10^{-4}, while graphene (E–Gr) further

https://doi.org/10.61577/jcti.2025.1000016

decreased wear to 0.72 × 10⁻⁴ and COF to 0.48 due to graphitic lubricity. The hybrid E–TiGr coating demonstrated the lowest wear rate (0.51 × 10⁻⁴) and COF (0.41), confirming the synergistic protective effect of TiO_2 and graphene.

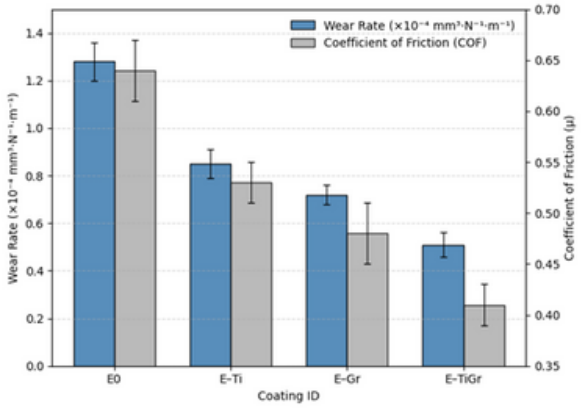

Figure 8. Variation in wear rate and coefficient of friction (COF) for E0, E–Ti, E–Gr, and E–TiGr coatings.

Electrochemical corrosion behavior (PDP and EIS analysis)

Electrochemical measurements were performed using an Autolab PGSTAT302N potentiostat in a three-electrode configuration with the coated sample as the working electrode, platinum as the counter electrode, and Ag/AgCl as the reference. A 3.5 wt.% NaCl solution simulated marine exposure. Potentiodynamic polarization scans were recorded from –1.5 V to +1.5 V at 1 mV·s⁻¹ after 30 min of OCP stabilization. As shown in Figure 9, the neat epoxy (E0) exhibited the most negative Ecorr (–0.782 V) and the highest icorr (3.9 × 10⁻⁶ A·cm⁻²), confirming poor barrier integrity. TiO_2 reinforcement (E–Ti) reduced icorr to 2.5 × 10⁻⁶ A·cm⁻², while graphene (E–Gr) further shifted Ecorr to –0.645 V and lowered icorr to 1.9 × 10⁻⁶ A·cm⁻². The hybrid E–TiGr coating showed the best corrosion performance, with Ecorr = –0.588 V and icorr = 1.1 × 10⁻⁶ A·cm⁻², corresponding to ~72% protection efficiency due to the compact, tortuous diffusion pathway created by the TiO_2–graphene network. For comparison, the neat epoxy coating (E0) is taken as the baseline with a protection efficiency of 0%.

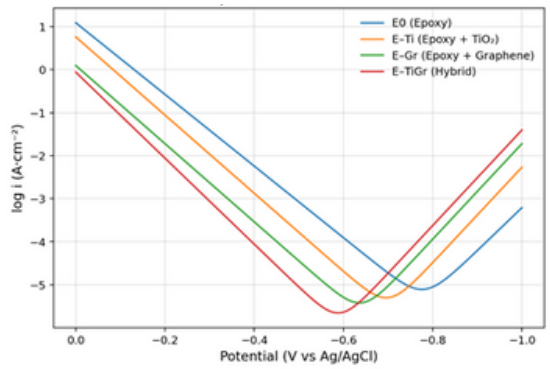

Figure 9. Potentiodynamic polarization (PDP) curves of E0, E–Ti, E–Gr, and E–TiGr coatings recorded in 3.5 wt.% NaCl solution.

EIS measurements recorded at open-circuit potential (10⁵–10⁻² Hz, 10 mV AC) produced Nyquist plots with semicircle diameters corresponding to charge-transfer resistance (Rct). The neat epoxy (E0) showed the smallest semicircle (~1.2 kΩ·cm²), while TiO_2 and graphene reinforcement increased Rct to ~2.5 and ~3.1 kΩ·cm², respectively [Figure 10]. The hybrid E–TiGr coating displayed the largest semicircle (~5.8 kΩ·cm²), indicating superior barrier integrity. Consistent with PDP results, E–TiGr also exhibited the most positive Ecorr (–0.588 V) and the lowest icorr (1.1 × 10⁻⁶ A·cm⁻²), confirming its strong resistance to ionic transport and corrosion initiation.

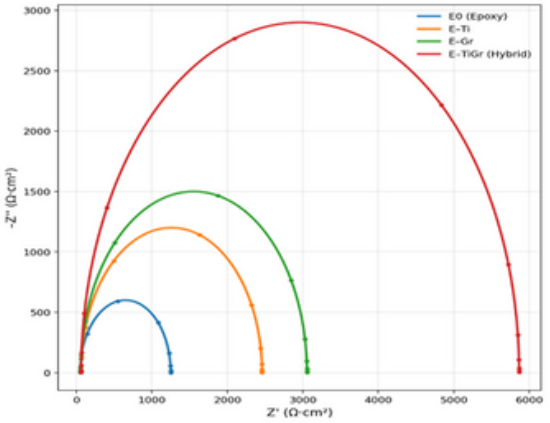

Figure 10. Electrochemical impedance spectroscopy (EIS) Nyquist plots of E0, E–Ti, E–Gr, and E–TiGr coatings in 3.5 wt.% NaCl solution.

These results align with, and in several aspects surpass, trends reported in earlier studies. TiO_2–epoxy coatings previously achieved only moderate corrosion improvements (icorr reductions of 30–40%) [1-3], while graphene–epoxy systems showed good barrier performance but were often limited by filler agglomeration [9, 14]. In contrast, the hybrid TiO_2–Graphene coating in this study achieved a markedly lower corrosion current density (1.1 × 10⁻⁶ A·cm⁻²) and the highest charge-transfer resistance (~5.8 kΩ·cm²). The enhanced hardness (42.1 HV) and reduced wear rate also exceed many single-filler epoxy reports [6-8], demonstrating the superior multifunctional synergy of the hybrid formulation.

Conclusions

The TiO_2–Graphene hybrid epoxy coating (E–TiGr) demonstrated the highest overall performance among all formulations evaluated in this study. The incorporation of 1.0 wt.% TiO_2 and 0.3 wt.% graphene increased the microhardness from 21.6 HV for neat epoxy (E0) to 42.1 HV, representing nearly a twofold enhancement. Tribological testing confirmed substantial improvements, with the wear rate decreasing from 1.28 × 10⁻⁴ mm³·N⁻¹·m⁻¹ (E0) to 0.51 × 10⁻⁴ mm³·N⁻¹·m⁻¹ for E–TiGr, accompanied by a reduction in the coefficient of friction from 0.64 to 0.41. Corrosion measurements in 3.5 wt.% NaCl further validated the superior protective behaviour of the hybrid coating. The corrosion potential shifted positively from –0.782 V (E0) to –0.588 V for E–TiGr, while the corrosion current density decreased from 3.9 × 10⁻⁶ to 1.1 × 10⁻⁶ A·cm⁻², corresponding to an overall protection efficiency of ~72%. Electrochemical impedance spectroscopy supported these findings, with the hybrid coating achieving the highest charge-transfer resistance (~5.8 kΩ·cm²) among all samples. Collectively, these values confirm that the TiO_2–Graphene hybrid reinforcement offers balanced and significant improvements in mechanical strength, wear resistance, and corrosion protection, making it a strong

https://doi.org/10.61577/jcti.2025.1000016

candidate for demanding service environments requiring long-term material reliability.

Disclosure Statement

The author declares that they have no known financial or personal conflicts of interest that could have influenced the work reported in this manuscript.

References

1. Chatterjee A, Islam MS. Fabrication and characterization of TiO_2–epoxy nanocomposite. Mater Sci Eng A. 2008;487:574–585. https://doi.org/10.1016/j.msea.2007.11.052
2. Huang KS, Nien YH, Chen JS, Shieh TR, Chen JW. Synthesis and properties of epoxy/TiO_2 composite materials. Polym Compos. 2006;27:195–200. https://doi.org/10.1002/pc.20173
3. Rubab Z, Afzal A, Siddiqi HM, Saeed S. Preparation, characterization, and enhanced thermal and mechanical properties of epoxy–titania composites. Sci World J. 2014;2014:515739. https://doi.org/10.1155/2014/515739
4. Sabzi M, Mirabedini SM, Zohuriaan-Mehr MJ, Atai M. Surface modification of TiO_2 nanoparticles with silane coupling agent and its effect on the properties of polyurethane composite coating. Prog Org Coat. 2009;65:222–228. https://doi.org/10.1016/j.porgcoat.2008.11.006
5. Mallakpour S, Barati A. Efficient preparation of hybrid nanocomposite coatings based on poly(vinyl alcohol) and silane-modified TiO_2 nanoparticles. Prog Org Coat. 2011;71:391–398. https://doi.org/10.1016/j.porgcoat.2011.04.010
6. Pinto D, Bernardo L, Amaro A, Lopes S. Mechanical properties of epoxy nanocomposites using titanium dioxide as reinforcement: A review. Constr Build Mater. 2015;95:506–524. https://doi.org/10.1016/j.conbuildmat.2015.07.124
7. Rahim-Abadi MM, Mahdavian AR, Gharieh A, Salehi-Mobarakeh H. Chemical modification of TiO_2 nanoparticles for encapsulation in polyacrylic shell via emulsion polymerization. Prog Org Coat. 2015;88:310–315. https://doi.org/10.1016/j.porgcoat.2015.07.013
8. Manap A, Mahalingam S, Vaithylingam R, Abdullah H. Mechanical, thermal and morphological properties of TPU composite reinforced by MWCNT and TiO_2 hybrid fillers. Polym Bull. 2020;:1–18. https://doi.org/10.1007/s00289-020-03393-z
9. Sanes J, Sánchez C, Pamies R, Avilés M-D, Bermúdez M-D. Extrusion of polymer nanocomposites with graphene and graphene derivative nanofillers: An overview. Materials (Basel). 2020;13:549. https://doi.org/10.3390/ma13030549
10. Vidakis N, Maniadi A, Petousis M, Vamvakaki M, Kenanakis G, Koudoumas E. Mechanical and electrical properties of 3D-printed ABS–graphene and carbon nanocomposites. J Mater Eng Perform. 2020;29:1909–1918.
11. Hanemann T, Szabó DV. Polymer–nanoparticle composites: From synthesis to modern applications. Materials (Basel). 2010;3:3468–3517. https://doi.org/10.3390/ma3063468
12. Mallakpour S, Madani M. Effect of KH550/KH570 coupling agents on nanostructure and interfacial interaction of ZnO/poly(amide–imide) nanocomposites. J Mater Sci. 2014;49:5112–5118. http://dx.doi.org/10.1007/s10853-014-8220-5
13. Li H, Zhang Z, Ma X, Hu M, Wang X, Fan P. Epoxy resin modified with nano-SiO_2 and γ-glycidoxypropyltrimethoxysilane: Synthesis and characterization. Surf Coat Technol. 2007;201:5269–5272. https://doi.org/10.1016/j.surfcoat.2006.07.143
14. Zhong F, He Y, Wang P-Q, et al. Graphene/V_2O_5@polyaniline ternary composites enable waterborne epoxy coating with robust corrosion resistance. React Funct Polym. 2020;151:104567. https://doi.org/10.1016/j.reactfunctpolym.2020.104567
15. Joseph Raj X. Electrochemical investigation into the effect of nano-titania on the protective properties of epoxy coatings on mild steel in natural seawater. Int J Petrochem Sci Eng. 2017;2(1):29–37. https://doi.org/10.15406/ipcse.2017.02.00028
16. Wang S-L, Zhu J-K, Rao Y-C, et al. Polydopamine modified graphene oxide–TiO_2 nanofiller for reinforcing physical properties and anticorrosion performance of waterborne epoxy coatings. Appl Sci. 2019;9(18):3760. https://doi.org/10.3390/app9183760
17. Khamme E, Sakulkalavek A, Sakdanuphab R. Anti-corrosion performance of vinyl ester resin films with titanium dioxide and graphene hybrid reinforcement. Mater Today Commun. 2022;33:104888. https://doi.org/10.1016/j.mtcomm.2022.104888
18. John S, Salam A, Baby AM, et al. Corrosion inhibition of mild steel using chitosan/TiO_2 nanocomposite coatings. Prog Org Coat. 2019;129:254–249. https://doi.org/10.1016/j.porgcoat.2019.01.025
19. Dou B-J, Xiao H, Lin X-Z, et al. Investigation of the anti-corrosion properties of fluorinated graphene-modified waterborne epoxy coatings for carbon steel. Coatings. 2021;11(2):254. https://doi.org/10.3390/coatings11020254
20. Zhou S-G, Wu Y-M, Zhao W-J, et al. Designing reduced graphene oxide/zinc-rich epoxy composite coatings for improving anticorrosion performance of carbon steel. Mater Des. 2019;169:107694. https://doi.org/10.1016/j.matdes.2019.107694
21. Vinodhini SP, Xavier JR. Evaluation of corrosion protection performance and mechanical properties of epoxy–triazole/graphene oxide nanocomposite coatings on mild steel. J Mater Sci. 2021;56(11):7094–7110. https://doi.org/10.1007/s10853-020-05636-w
22. Chandraraj SS, Xavier JR. CuO-anchored graphene oxide for enhancing mechanical and anticorrosion properties of epoxy coatings in cooling water systems. Mater Chem Phys. 2023;305:127953. https://doi.org/10.1016/j.matchemphys.2023.127953
23. Zhang L-S, Zhang P-B, Shen L-M, et al. Modified graphene oxide/waterborne epoxy composite coating with enhanced corrosion resistance. Prog Org Coat. 2022;172:107100. https://doi.org/10.1016/j.porgcoat.2022.107100
24. Zhou Z-Y, Ji X-H, Pourhashem S, et al. Investigating the effects of g-C_3N_4/graphene oxide nanohybrids on corrosion resistance of waterborne epoxy coatings. Compos Part A Appl Sci Manuf. 2021;149:106568. https://doi.org/10.1016/j.compositesa.2021.106568
25. Xu QF, Liu Y, Lin F-J, Mondal B, Lyons AM. Superhydrophobic TiO_2–polymer nanocomposite surface with UV-induced reversible wettability and self-cleaning properties. ACS Appl Mater Interfaces. 2013;5(21):8915–8924. https://doi.org/10.1021/am401668y

https://doi.org/10.61577/jcti.2025.1000016

26. Al-Turaif HA. Effect of nano TiO_2 particle size on mechanical properties of cured epoxy resin. Prog Org Coat. 2010;69(2):241–246. https://doi.org/10.1016/j.porgcoat.2010.04.004

27. Taheri N, Hashemi H, Soroush E, Afsahi P, Ramezanzadeh B. $Ti_3C_2T_x$ MXene/MoS_2 hybrid nanocomposites for synergistic smart corrosion protection of epoxy coatings. J Colloid Interface Sci. 2025;682:894–914. https://doi.org/10.1016/j.jcis.2024.11.205

28. Cai M, Feng P, Yan H, Li Y, Song S, Li W, et al. Hierarchical $Ti_3C_2T_x$@MoS_2 heterostructures: a first principles calculation and application in corrosion/wear protection. J Mater Sci Technol. 2022;116:151–160. https://doi.org/10.1016/j.jmst.2021.11.026

29. Zambrano-Mera DF, Broens MI, Villarroel R, Espinoza-Gonzalez R, Aguilar-Hurtado JY, Wang B, et al. Solid lubrication performance of sandwich Ti3C2Tx-MoS2 composite coatings. Applied Surface Science. 2023;640:158295. https://doi.org/10.1016/j.jmst.2021.11.026

30. An D, Wang Z, Qin L, Wu Y, Lu S, Yang H, et al. Preparation of MXene/epoxy coating for promising anticorrosion and superlow friction properties. Prog Org Coat. 2023;183:107779. https://doi.org/10.1016/j.porgcoat.2023.107779

https://doi.org/10.61577/jcti.2025.1000016